

New time-domain model for active mode locking, based on the transmission line laser model

A.J. Lowery, PhD, AMIEE

Indexing terms: Lasers, Transmission lines, Modelling

Abstract: A new time-domain model for active mode-locking in semiconductor lasers, coupled to external cavities including a filter, is developed. Unlike previous time domain models, the propagating field is considered, rather than the photon density. This allows time-domain filters to be used to model the spectral dependencies of gain, spontaneous emission and dispersive components. Also, Fourier transforms of the field reveal the output spectrum.

The new model is compared with results from a previous time-domain model before the effects of bandwidth limiting on pulse shape are investigated. Results show that transform limited pulses can be generated. However, their stability is critically dependent on the drive conditions and the spontaneous emission coupled to the lasing mode.

1 Introduction

Mode locking in semiconductor lasers can be divided into two areas, passive mode locking, and active mode locking. Passive mode locking requires a saturable absorber element within the round trip path of the light [1]. This paper concentrates on active mode locking of lasers coupled to a dispersive external cavity, where the laser gain is modulated via its injection current at frequencies near to the external cavity's resonance [2]. This method has recently been used to generate pulses with widths less than 1 ps at repetition rates of a few GHz [3]. Active mode locking promises to provide the stable, narrow linewidth pulses required for optical time division multiplexed (OTDM) systems, operating at data rates of hundreds of Gbit/s [4].

Harris first attempted active mode locking using semiconductor lasers [5], and Ho *et al.* achieved successful locking in 1978 [6]. Mode locking implies that the relative phases of the individual resonator modes are fixed. This allows very short, transform limited pulses to be generated. The minimum pulse width possibly achievable is of major interest.

Several theories are available which give the pulse width, most providing an analytical expression together with necessary assumptions [7-14]. However, Aspin and Carroll [15], and Demokan [16] have developed numerical methods in the time-domain. These offer more insight into the transient development of a mode locked pulse

train, but are unable to model the spectral dependencies within the device, or the spectral composition of the output pulse train if dynamic changes in the refractive index are included.

Kempf and Garside [17], Chen and Pan [12] and van der Ziel [13] have also developed time-domain models. However, these are noniterative, assuming that the pulse profile is reproduced exactly after one round trip of the cavity (known as a 'self-reproducing profile'). The results of this model will show that this may not be the case as long term variations take place as the pulse evolves. The self reproducing profile approach has also been used in some frequency domain models, as it allows the resulting periodic waveform to be transformed to a discrete set of Fourier coefficients [18]. Dynamic models have also been developed for solid state lasers [1, 19].

This paper presents a model which may appear similar to Demokan's; indeed, it has all the advantages described in his paper [16]. However, the important difference is that the propagating field is modelled, rather than the propagating photon density. As stressed in his paper, the photon density equations contain no phase information. Aspin and Carrolls' paper was criticised for this reason [10, 16].

The absence of phase information means that the equations cannot be used to model dispersive cavities, such as those with grating filters. Also, the spectral dependencies of gain or spontaneous emission cannot be modelled. With pulse widths wider than a picosecond, the effect of the laser gain's spectral dependence will be negligible. However, the spectral dependence of the spontaneous emission caused by the Fabry-Perot modes may be important.

Modelling the propagating field allows the spectral dependencies to be included without a great increase in the computational task. Also, the results may be easily converted from the time-domain to the frequency by means of Fourier transforms. This may be particularly important if the model is to be expanded to include dynamic changes in refractive index which modulates the optical phase. However, techniques are required to represent the optical components and emission processes as modifiers to the field. Also, a suitable sampling interval for the field has to be chosen so that the computational task does not become excessive or the model inaccurate.

Fortunately, a time-domain technique called the Transmission Line Laser Modelling (TLLM) method is readily adaptable to mode-locked lasers [20-23]. This is based on the Transmission-Line Matrix (or Modelling) method (TLM), which was originally developed for the modelling of fields in microwave components using a mesh of transmission lines as a thought step between reality and a computer algorithm [24]. The TLLM produces algorithms with a topology in correspondence with

Paper 6876J (E13), first received 31st March and in revised form 21st July 1989

Dr. Lowery is with the Department of Electrical and Electronic Engineering, University of Nottingham, University Park, Nottingham NG7 2RD, United Kingdom

the physical device. This allows for quick development of algorithms for new device structures. The transmission lines serve to connect scattering nodes and to provide distortionless transmission of pulses but with a fixed time delay. The scattering nodes 'scatter' incident pulses which become reflected pulses, from the lines back into the lines. These new pulses then take exactly one iteration timestep to cross the connecting lines to become new incident pulses on adjacent nodes. The process then repeats until the problem is solved. The purpose of the lines is to model the propagation of the waves, and to break the problem into small parts which may be solved independently at each iteration.

It is the form of the scattering which defines the physical problem to be solved. In transmission line laser modelling, scattering nodes are provided for:

- (a) the material gain loss and spontaneous emission processes along the laser cavity
- (b) reflectivity and externally transmitted waves at the facets
- (c) propagating waves in external resonators
- (d) optical filters

This paper will describe how such nodes are connected together to form an actively mode locked laser model.

As mentioned above, the key advantages of Demokan's model are retained in this new model. These include:

- (a) No assumption about the pulse shape. The pulse is allowed to develop from noise as it would in a true device that had been just turned on.
- (b) Gain-saturation effects included. Many models assume that the gain follows the input current. However, gain saturation may be significant.
- (c) The model allows for inhomogeneous gain in the laser cavity. Demokan showed this to be important, as the gain varies by up to 5% along the cavity.
- (d) Spontaneous emission noise correctly treated [21].

The transmission-line laser model treats spontaneous emission as a random current source injecting into the transmission lines. This is an exact analogue of the current density vector model used by Marcuse to calculate the spontaneous emission coupling factor. It is also spectrally correct as the spontaneous power becomes concentrated around the cavity's resonances as the Q is increased. An added advantage of this model is that the random noise allows the stability of the pulses to be studied.

However, the following approximations are common to both models:

- (a) Only a single transverse mode is modelled. This allows a one-dimensional treatment to be used.
- (b) Diffusion is neglected in all directions. However, diffusion can be modelled in the longitudinal direction using the TLLM as it could be using Demokan's model.
- (c) Homogeneous current injection is assumed. However, longitudinal variations can be modelled with the TLLM and Demokan's model, making them ideal for multi-contact devices.
- (d) Homogeneous light intensity distribution in the transverse and lateral directions. This is a consequence of the one-dimensional, single transverse mode, treatment.
- (e) The change in the real part of the refractive index with electron density is neglected. This is not a fundamental limitation of the TLLM [22].
- (f) Dispersion within the laser medium is ignored. However, this model includes the dispersion of the grating filter in the external cavity.

2 Model theory and development

A typical external cavity laser capable of mode locked operation is shown in Fig. 1A [25-33]. It consists of a laser chip with a reflection coated front facet, to give

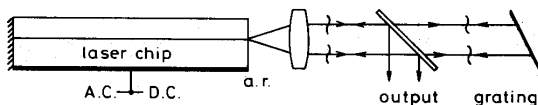


Fig. 1A A mode-locked laser system

nearly 100% reflection, and an antireflection coated rear facet, to give nearly 100% transmission. The rear facet is coupled into an external cavity comprising an anti-reflection coated coupling lens, an angled half-silvered mirror to couple some of the light to measuring instruments, and a ruled diffraction grating to select the operating wavelength and bandwidth of the device. The grating is thought to reduce the spontaneous emission noise and so aid stable mode locking [7].

The model for such a device consists of a standard Fabry-Perot TLLM [20] with additional external components to simulate the external cavity, as shown in Fig. 1B. These components serve to delay the sampled waves

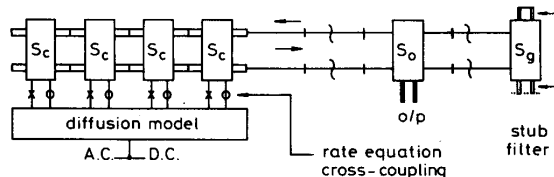


Fig. 1B Transmission line representation of a mode-locked laser system

Scattering matrices S_c represent the laser chip, matrix S_o represents the output mirror, matrix S_g represents the grating. The diffusion model for carriers determines the gains of the matrices S_c and accounts for carrier recombination by stimulated and spontaneous emission

from the laser chip model, then return them to the laser chip model attenuated and filtered. It is convenient to break the model down into four sub-models relating to the components that make up the physical device. These are described in detail below.

2.1 Laser chip model

In most TLLMs the material gain and spontaneous emission spectral dependence over a number of modes are modelled. However, in this model, the dispersive grating is assumed to dominate the spectral characteristics. This means that the filter circuits associated with the above dependencies may be ignored. Thus, stimulated emission is simply modelled by amplifiers along the length of the laser chip, and spontaneous emission by unfiltered white noise sources. Waveguide scattering losses are simply modelled by attenuators. The relation between a wave passing into a modelling section, represented by a voltage pulse, ${}_cV^i$, and a wave leaving the section, ${}_cV^r$, of length ΔL , is

$${}_cV^r = {}_cV^i \exp [\Delta L \Gamma a (N(n) - N_0)/2 - \Delta L \alpha_{sc}/2] + I_s \Delta L Z_p/2 \quad (1)$$

where Γ is the optical confinement factor, a the gain cross-section, $N(n)$ the carrier density in section n , N_0 the transparency carrier density, α_{sc} the scattering loss per

unit length, Z_p the cavity wave impedance [20] and I_s the random current injected per unit length (representing spontaneous emission) whose mean-square value is [21]

$$\hat{I}_s^2 = 2\beta[N(n)]^2 B h f s, m^2 / (\Delta L Z_p) \quad (2)$$

where β is the spontaneous coupling factor per laser chip mode, hf is the mean energy of emitted photons, s is the number of sections used to model the laser chip, m is a unity constant with units of metres, and B is the bimolecular recombination constant.

The waves are simply passed between the sections on transmission lines which serve to model the propagation delay along the cavity. Eqn. 1 is applied to the waves as they pass in both directions through a section. During each iteration, the carrier iteration is recalculated using a discrete time approximation to the carrier density rate equation, given by

$$\begin{aligned} k_{+1}N(n) = & kN(n) + \Delta T [I/(wdLq) - [I_k N(n)]^2 B \\ & - a\Gamma c_k S(n)(kN(n) - N_0)/\bar{n}_e] \quad (3) \end{aligned}$$

where $kN(n)$ is the carrier density for the k th iteration, $k_{+1}N(n)$ that for the $(k+1)$ th iteration, I the injection current to the whole laser, wdL the laser's active volume, c the velocity of light and \bar{n}_e the group effective index of the waveguide.

The iteration time step is linked to the section length by the velocity in that section, i.e.

$$\Delta T = \Delta L \bar{n}_e / c \quad (4)$$

The photon density within a section, $S(n)$ is related to the wave amplitudes incident on the section from both sides by

$$S(n) = \bar{n}_e ([\tilde{V}^i]^2 + [\tilde{V}^r]^2) / (Z_p h f c m^2) \quad (5)$$

The front facet simply reverses the direction of the waves incident upon it, however, the rear facet couples to the external cavity which has delay, loss and dispersion.

2.2 External cavity model

The easiest way to simulate the external cavity's delay is to store the sampled optical waveform pulses in consecutive elements of an array. The pulses may then be retrieved after an appropriate number of iterations.

Ideally, the filter and coupling mirror should be placed halfway along the delay. However, to minimise the computational task, the models of these components were placed just before the wave enters the rear facet. This means that only a single delay is required, rather than one for each light path between each component. This approach does not affect the results.

2.3 Filter model

The filter was modelled using a transmission line stub equivalent of a bandpass RLC filter, similar to those used to model the spectral dependence of gain in the first TLLM. The stub filter, which is placed between the cavity delay model and the laser chip model and operates on waves entering the laser chip model, is shown in Fig. 2.

The equations governing the scattering of pulses incident on the filter's node can be obtained by treating each transmission line by its Thévenin equivalent, also shown in Fig. 2. The potential at the connection node, v , which is the output voltage, cV^i , of the filter is

$$v = (cV^r + 2V_L^i Y_L + 2V_C^i Y_C) / (1 + Y_L + Y_C) \quad (6)$$

where cV^r is the incident voltage from the delay lines which is assumed to be buffered to avoid reflections, V_L^i is the incident voltage from the inductive stub of admittance Y_L and V_C^i is the incident voltage from the capacitive stub of admittance Y_C . Equations fixing the admittances are given in [20].

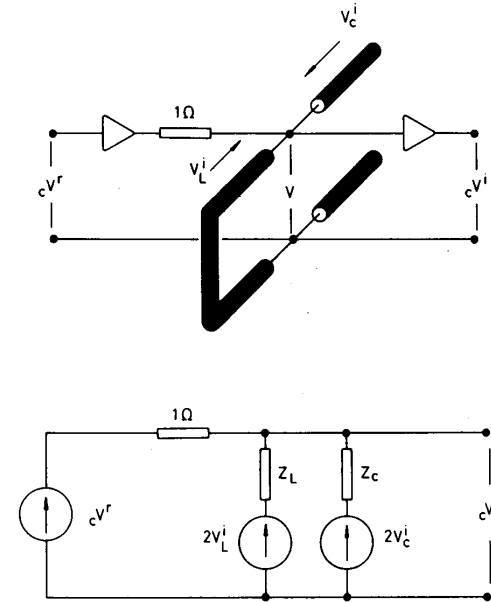


Fig. 2 The stub filter representing the grating (top), together with its Thévenin equivalent circuit (bottom)

The inductive and capacitive stubs are one-half a timestep in length. This means that pulses reflected into them from the scattering node will return to the node as incident pulses after one timestep. Using the fact that the sum of incident and reflected voltages at the node-ends of the stubs sum to the potential of the node, and that the pulses are reflected at the opposite ends of the stubs the new incident pulses can be related to the previous incident pulses by

$$\begin{aligned} k_{+1}V_L^i &= kV_L^i - kv \quad (\text{for the inductive stub}) \\ k_{+1}V_C^i &= kv - kV_C^i \quad (\text{for the capacitive stub}) \end{aligned} \quad (7)$$

Theoretically, this filter has a Lorentzian response. However, the limited bandwidth of the model, set by the iteration timestep, truncates the response as is shown in Fig. 3. Note how the modelled response a good fit to the Lorentzian curve around the pass-band peak. Better fits to the grating response could be obtained using either a multipole filter or a multistage digital filter. This is beyond the scope of the present paper.

2.4 Coupling mirror model

The coupling mirror and the cavity losses can be simply represented by a frequency independent scattering matrix, placed just before the rear facet. The voltage pulses, from the rear facet and representing the optical field, can be converted to optical power from the output coupling mirror using the following equation

$$P = |cV^r|^2 wdC / (Z_p m^2) \quad (8)$$

where wd is the cross sectional area of the active region and C is the coupling efficiency of the output mirror

(ratio of output power to power exiting the rear facet of the laser). Note that for this calculation all the optical power is assumed to travel inside the active region. This

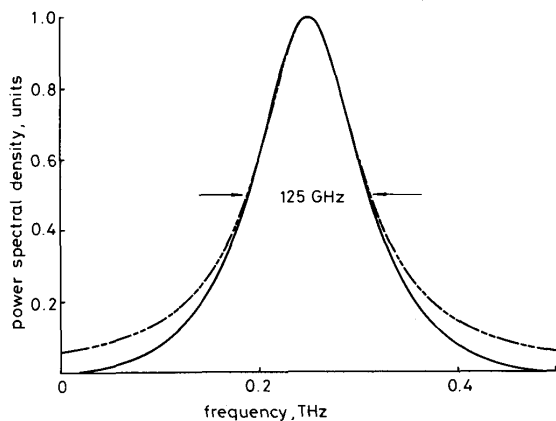


Fig. 3 The response of the stub filter together with the theoretical response of an RLC filter (Lorentzian)

Note the truncation of the model's response at the extremes of the modelled bandwidth
 — model
 - - - Lorentzian

does not affect the validity of using a confinement factor to modify the gain term in eqn. 1.

2.5 Choice of timestep

In all TLLMs, the computer time required to model a fixed amount of laser time is proportional to the inverse of the timestep-squared. This is because the number of longitudinal model sections increases inversely with the timestep. This is true with the proposed model, except that the external cavity adds a small overhead proportional to the inverse of the timestep.

In previous models, the frequency selective element has been the gain-curve. To accurately model this has required a small timestep, to give a large bandwidth. Interestingly, the bandwidth, measured in longitudinal modes, is always equal to the number of sections along the laser chip. For a mode-locked device, the system bandwidth is dominated by the dispersive element. This is typically a hundred GHz, much less than that of the material gain. This allows a much larger timestep to be used for mode locked lasers, hence fewer sections. This is fortunate, as most mode locked lasers require tens of round trips to reach a stable state and a short timestep would mean a large computational task. In these simulations, 1 ns of laser time took about 35 seconds of computer time on a small (32016) workstation. However, the program was not optimised for mode locked lasers. Indeed, it could be used for all TLLM models. The program required storage for less than 1000 real numbers.

The timestep used here was 1 ps, giving a model bandwidth of 500 GHz. The dispersive element had a FWHM bandwidth of 125 GHz. In comparison, Demokan used timesteps of 1 ps and 0.25 ps. It is expected that his model had a similar run time per modelled nanosecond, because the algorithms are similar apart from Demokan modelling photon density, and the TLLM modelling field. The only extra complexity of this model is the dispersive filter, some random number generation and some equations to convert the photon rate equations to one for field. It is

therefore interesting to ponder on the advantages gained by simply changing the modelled variable from photon density to field: the effects of the filter and noise on the output spectrum can be sought without significantly increasing the computational task.

Demokan saw a stable pulse develop, from a single oscillating mode, under certain conditions, in around 100 round-trips. Aspin and Carroll used a similar number of trips and showed the development of double pulses. These large numbers, requiring many iterations in an accurate mode, have put many people off using an evolutionary modelling method [18], and made self-consistent-profile (SCP) methods popular. However, these are unable to show the stability of any pulses, and in most cases, place assumptions on the pulse's shape. In any case, an evolutionary approach is more akin to reality.

3 Results

Table 1 gives the laser's parameters. These are equivalent to those used by Demokan, where possible. However, some parameters require explanation:

Table 1: Laser parameters

Symbol	Parameter name	Value	Unit
λ_0	gain-peak wavelength	851.064	nm
L	laser cavity length	300	μm
L'	external cavity length	5	cm
w	active region width	5	μm
d	active region depth	0.15	μm
Γ	optical confinement factor	0.5	
\bar{n}_g	laser group effective index	4.0	
N_0	transparency carrier density	1.2×10^{18}	cm^{-3}
a	laser gain constant	5.33×10^{-18}	cm^2
α_{sc}	total laser cavity attenuation	13.365	cm^{-1}
R_f	laser front facet reflectivity	1.00	
R_o	external cavity reflectivity including coupling loss	0.21	
B	radiative recombination coef.	4.0×10^{10}	cm^3/s
β	effective spontaneous coupling factor per laser mode	1×10^{-4}	
c	vacuum velocity of light	3×10^{10}	cm/s
s_l	number of laser model sections	4	
S_o	number of external cavity sections	166	
b	model bandwidth	353	
Δf	dispersive filter bandwidth (FWHM)	125	GHz
I_{dc}	DC bias current	26.622	mA
I_{ac}	AC drive current (zero-peak)	13.05	mA
I_{th}	calculated threshold current	26.1	mA

(a) The spatial gain coefficient, a , is Demokan's optical gain coefficient, g , divided by the group velocity along the cavity.

(b) The total cavity attenuation factor, α_{sc} , is from Demokan's eqn. 4, with a carrier density of $1.346 \times 10^{18} \text{ cm}^{-3}$.

(c) The spontaneous emission factor per laser chip mode, β , is a factor of four smaller than was calculated from Demokan's factor per external cavity mode, $k\Gamma$. This is to prevent the spontaneous emission noise from causing excessive amplitude jitter but was found to have little effect on the pulse widths.

The results concentrate on the effects of altering

- the RF drive frequency (the detuning),
- the spontaneous emission coupling to the cavity modes,
- the DC bias level,
- the AC drive current,
- the grating filter bandwidth.

3.1 Effect of detuning

In this paper, the detuning is defined as the RF drive frequency minus the inverse of the cavity round trip time. The delay due to the grating dispersion was included in the round trip. This is $1/(\pi\Delta f)$ seconds for a grating bandwidth of Δf FWHM.

Detuning is thought to improve pulse stability and minimise pulse width [14, 16, 18] and this has been shown experimentally [13, 25, 26]. To investigate this, five different RF drive frequencies were used, and the temporal evolution of the pulses examined. The pulse evolution for the first 32 pulses with a near-optimum detuning of 4.67 MHz is shown in Fig. 4A. Fig. 4B shows

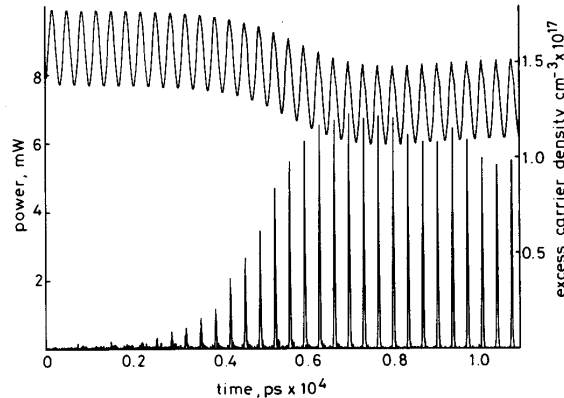


Fig. 4A Build up of mode locked pulses for optimum detuning ($f_r - f_c = 4.67$ MHz) and under the conditions in Table 1 when AC Drive is first applied to the device

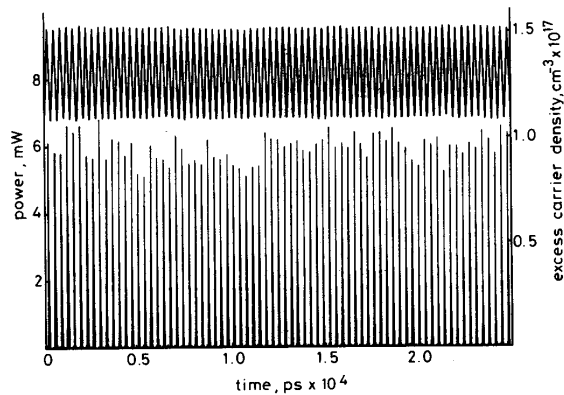


Fig. 4B Stability of the pulses after 400 ns. Every sixteenth pulse is plotted, i.e. the plot represents 400 ns of laser time

every sixteenth pulse 1170 pulses into the simulation. This shows that, whilst there are random variations in pulse amplitude because of the random spontaneous emission, there are no periodic variations indicating incorrect detuning. Note that the use of boxcar integration to obtain experimental results masks pulse to pulse variations and that further reduction of the spontaneous coupling factor in the model gives more stable pulses.

The growth of the pulses from noise was rapid (Fig. 4A), at around 20 round trips. This compares to around 170 round trips in Demokan's simulations. However, it should be noted that his pulses evolved from a single oscillating mode and that no bandwidth limi-

tation was used. Interestingly, AuYeung *et al.* have observed pulse growth within 20 round trips of applying the RF drive [27].

The pulses are shown to peak just before the unsaturated peak of the average carrier density waveform, but after the peak when the carrier density is saturated. This is in contrast to Demokan's result, however, it is in agreement with [14, 18].

The pulses in this simulation had almost linear sides and little broadening at their bases (Fig. 5A) whereas

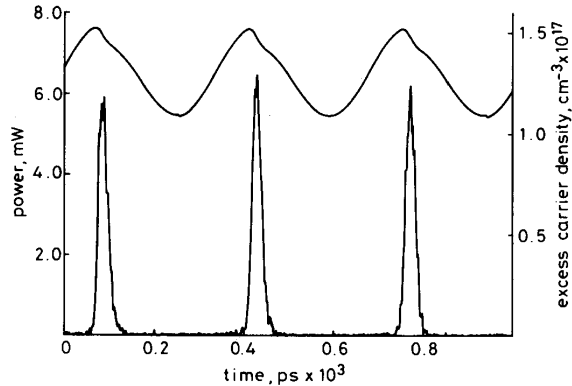


Fig. 5A Three pulses of Fig. 4B in detail

Demokan's pulses have a slow initial rise and a definite pedestal after the initial peak. The TLLM pulses appear consistent with pulses recorded by means of streak cameras [26, 28, 31].

The average pulse width (FWHM) was around 22 ps in this simulation and 16 ps in Demokan's. This discrepancy is probably caused by the inclusion of a filter in this model. The peak power out of the laser facet next to the external cavity varied (because of the random noise source) around 20 mW (6 mW after the coupling mirror). This compares with 8.61 mW in Demokan's work ($S(l_s, t) = 6.55 \times 10^{14} \text{ cm}^{-3}$). Because of the differences in pulse shape, the pulse energies in both simulations are expected to be similar.

The use of the TLLM technique allows the laser's spectrum to be examined using Fourier transforms of the field. Fig. 5B shows the spectrum after the laser has stabilised. This is composed of the cavity resonant modes,

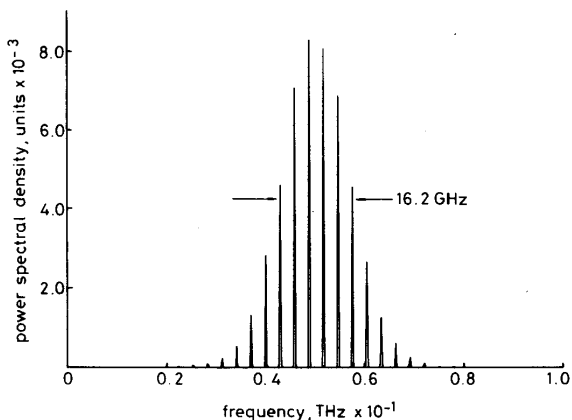


Fig. 5B The spectrum of the pulses in Fig. 5A

spaced at the drive frequency, enclosed within a Gaussian-like bell with a width of 16.2 GHz. The well defined peaks indicate that the modes were phase locked over many pulses.

The time bandwidth product (TBP) was around 0.36 which implies transform limited pulses. For comparison, Gaussian pulses have a TBP of 0.44 and Sech² pulses a TBP of 0.315. Experimental work has produced TBPs of 0.3 [28], 0.38–0.5 [3], <0.42 [29], 0.44 [30], 0.46 [31, 32], and 0.58 [33]. However, it must be remembered that some of these results are from autocorrelation measurements where the pulse shape has to be guessed and others are averaged pulse-shapes which may have been broadened because of jitter.

In contrast, Demokan claimed that his pulses were not transform-limited. However, he did not obtain the pulse spectra to find the bandwidth, but used the system bandwidth, which was unlimited. Thus, he deduced that the time-bandwidth product was large.

When the RF drive frequency was increased (greater detuning) the pulse height and pulse shape became unstable and both varied in a cyclic manner. Fig. 6 shows

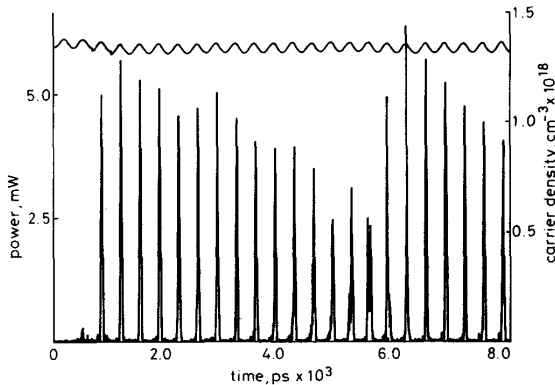


Fig. 6 The effect of increasing the RF drive frequency (detuning = 13.2 MHz), on pulse stability, showing the evolution of prepulses which become the main pulses

the pulse evolution for 13.2 MHz detuning with every eighth pulse plotted. The initial build-up was similar to that of the optimum detuning. However, after a real time of 32 ns (marked 4 ns) a prepulse began to build up. After 46 ns (5.7 ns) this prepulse became dominant and the initial main pulse began to die away. The simulation was run for over 2300 pulses and this prepulse build up and eventual domination repeated in a cyclic manner.

An explanation for this behaviour is that a high RF drive frequency causes the circulating optical pulse to slip after the time for peak gain. Thus the gain favours the growth of a new pulse at its peak. After a while this new pulse slips to behind the time of peak gain. Thus, the process is periodic.

A plot of the minimum pulsewidth versus the detuning appears in Fig. 7. At high applied frequencies, prepulses appear cyclically (points marked 'a'). At low applied frequencies postpulses appear cyclically (points 'c'). At frequencies near to optimum detuning (points 'b') stable pulses are produced and their width is a function of the detuning. In comparison, experimental results have shown that the pulse width is very sensitive to detuning [13, 25, 26]. However, it is difficult to make accurate comparisons because most experimental results average over many pulses so that the cyclic behaviour is not

observed, and the reference for zero detuning is difficult to establish.

3.2 Effect of spontaneous emission noise

Demokan's model predicted that the main determinant of pulse-width was the amount of spontaneous emission.

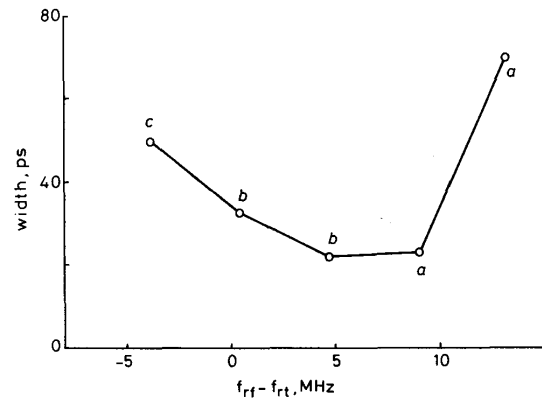


Fig. 7 Plot of the minimum pulse width versus the RF detuning (modulation frequency minus cavity resonance frequency)

'a': pre-pulse build-up 'b': stable pulses 'c': post-pulse build-up

However, his model did not include a dispersive element. Also, the noise was scaled to be inversely proportional to the pulse width and proportional to the spectral width. This may not have been a correct assumption, as the spectral distribution of the noise is a complex function of the cavity loss and the noise in many non-oscillating modes may have an effect because of coupling between the modes via the carrier density [21]. His assumption that the coupling factor is inversely proportional to the laser chip length is also suspect, mainly because the laser is AR coated and exists within an external cavity.

Simulations for five different coupling factors are shown in Figure 8. For low noise inputs the pulse inten-

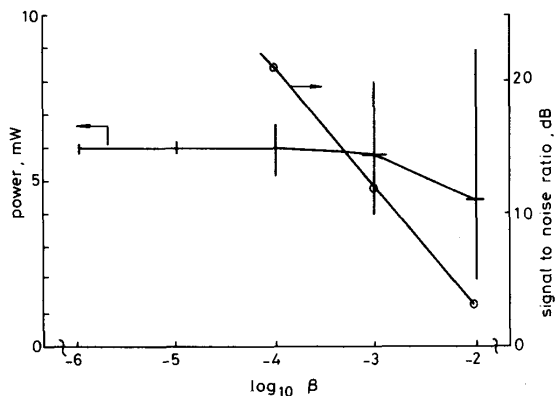


Fig. 8 Effect of spontaneous coupling per cavity mode on pulse power and signal-to-noise ratio

Note the increasing uncertainty in pulse power as the noise coupling is increased

sity is very stable. However, as the noise is increased, the pulse intensity fluctuates. However, the pulse widths remain essentially the same, except for coupling factors over 1%, where noise has drowned any attempt at producing mode-locked pulses. In contrast, Demokan

showed a large variation in pulse-width (nearly an order of magnitude) for a fifty times increase in coupling. This may be because of the non-random nature of his noise source: the random nature of the TLLM source may make it less likely for a pulse to build up before the gain has reached its peak.

3.3 Effect of DC drive level

Demokan showed that the laser's behaviour was critically dependent on the DC bias level. For example, increasing the bias reduced the pulse width, but at levels above $1.04 \times$ the threshold current, double peaked pulses were produced and pulse stability suffered. Simulations using this model showed a similar behaviour, but the pulses remained stable over a greater range of currents.

Fig. 9 plots the variations in pulse width and peak power against bias current. At levels below the threshold

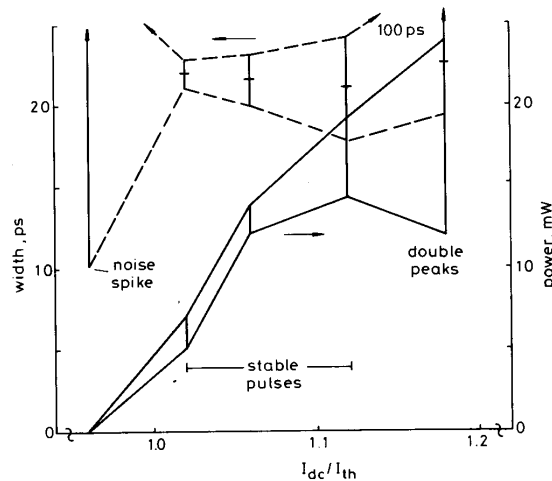


Fig. 9 Effect of DC bias current on pulse width and pulse power

The most stable pulses, in terms of amplitude and width, are obtained at bias levels just above threshold

current the output power was extremely small (as shown by Demokan). The pulses were swamped by noise which was modulated at the drive frequency. The widths of pulses were difficult to define. However, it was possible to measure noise spikes down to 5 ps. Measurements of such spikes in an experimental situation would, of course, be erroneous.

At levels between 1.02 and $1.12 \times$ threshold the pulses were stable and single-peaked. Increasing bias decreased the mean pulse width slightly and increased the pulse power, in agreement with Demokan. However, the uncertainty in these values was also increased.

At levels around $1.18 \times$ threshold the pulses gained double peaks in a cyclic fashion. The double pulses had a FWHM of over 100 ps and the peak pulse power dropped to maintain a nearly constant pulse energy. Obviously, operation at these levels would be undesirable because of the large pulse position and amplitude jitter and large pulse widths.

3.4 Effect of AC drive level

Demokan has also shown that the AC (RF) drive level has similar, albeit less severe, effects on the pulses as did the DC bias level. This model also predicted that the pulse width can be reduced and the peak power increased with increasing AC drive, as shown in Fig. 10. However,

it appears that the minimum pulse width is limited, probably by the grating, so that no benefit is gained by increasing the drive above the $0.5 \times$ threshold current.

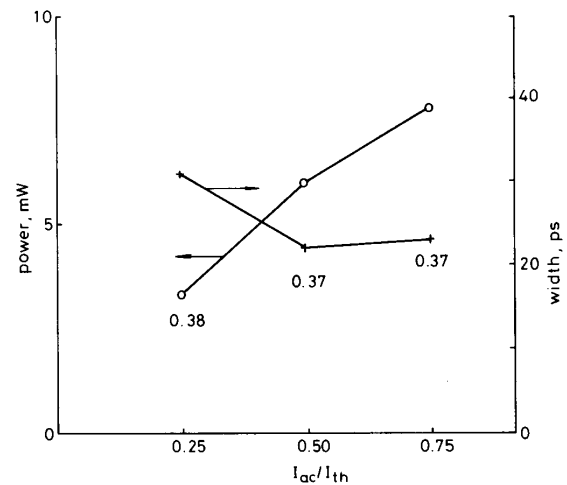


Fig. 10 Effect of AC drive current on pulse width and pulse power

The labels are the time-bandwidth product averaged over six pulses

Double pulsed generation has not been seen. However, the trailing edges of the pulses become slower than the leading edges as the drive is increased. It is interesting to note that the time bandwidth product of the pulses remains essentially constant at all drive levels.

3.5 Effect of grating bandwidth

The AC drive simulations above suggest that the grating limits to which the minimum pulse-width is obtainable, are around 20 ps. To test this theory, the Q of the grating filter was reduced to increase its bandwidth and the model run with the parameters in Table 1.

With a bandwidth of 330 GHz the pulsewidth was reduced to 10.6 ps. Pulses from this simulation are shown in Fig. 11A. The pulses are asymmetrical with leading

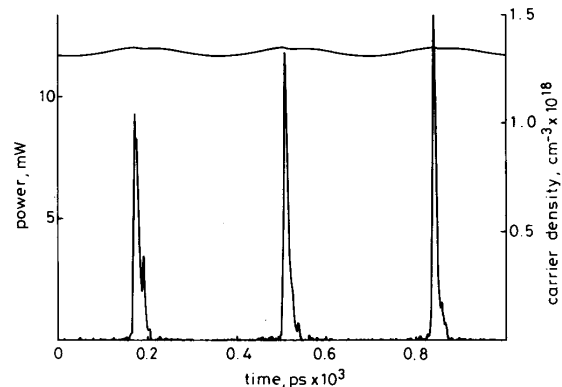


Fig. 11A Mode-locked pulses when the grating bandwidth is increased to 330 GHz

edges and slow, ragged trailing edges. The spectrum over eleven pulses is shown in Fig. 11b. This had a FWHM of 28 GHz, giving a TBP of 0.30 which is in agreement with experimental results from Vasil'ev who also obtained asymmetrical pulses but at higher drive levels [28]. The

tails in the spectrum may be a result of an increased level of spontaneous emission because of the greater filter bandwidth. They could also be a result of the filter

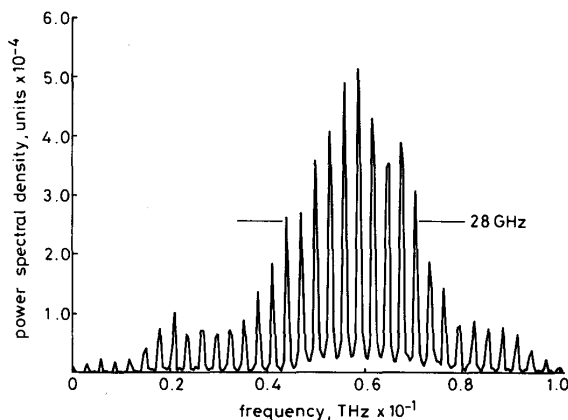


Fig. 11B Spectrum of the mode locked pulses using a 330 GHz grating

response modified because of the limited model bandwidth. However, this effect has been observed experimentally [34]. Note that the peak of the spectrum does not lie at the centre of the grating's pass-band. This implies an unstable operating wavelength which may have important system consequences.

A plot of pulse width versus the reciprocal of grating bandwidth is shown in Fig. 12. In each case the detuning

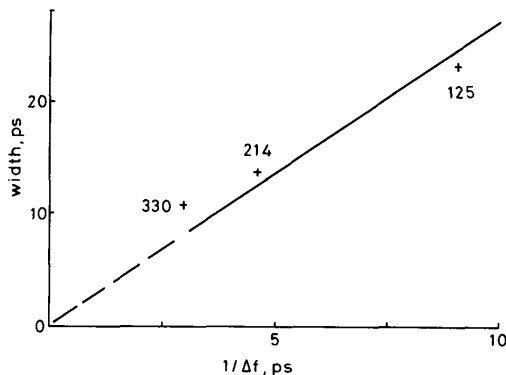


Fig. 12 Pulse width versus the reciprocal of grating bandwidth, GHz

was optimised for optimum pulsewidth. This graph suggests that a wide-bandwidth grating should be used for minimum pulse widths. However, the ultimate pulse width may be limited by either spontaneous emission noise, reflections from the coated laser facet, dispersion from the grating, or laser chirp.

4 Conclusions

A new model for mode-locking in dispersive external cavities has been developed by simple modification of the transmission line laser model. The model produces results in qualitative agreement with those of a previous time-domain model. An advantage of this new model is

that spectral dependencies have been included, such as those of the grating and of the resonant cavity.

The model shows that detuning, DC drive, AC drive, spontaneous coupling and grating bandwidth are all important to the pulse width, pulse stability and output power. In all cases the pulses were transform limited, the time bandwidth product being 0.36 for symmetrical pulses produced with a narrow system bandwidth and 0.3 for asymmetrical pulses produced using a larger system bandwidth. In this second case, the output spectrum had side lobes. The ability to predict the spectrum is an important advantage of this new model over a previous time-domain model.

Because the model is such a close representation of the physical device, it is easy to modify it to include more detail. For example, it would be interesting to investigate the effects of non-perfect antireflection coatings on the facet and lens. Also, the effect of carrier induced refractive index change would be interesting to model as it may lead to a chirped or spectrally shifted output. This would be difficult using models neglecting phase.

The model may be also linked to an existing model of a travelling wave laser amplifier. This could be used to simulate power boosted OTDM transmitters. Of particular interest would be the effect of amplifier dynamic gain saturation on the pulse shape.

5 References

- NEW, G.H.C.: 'The generation of ultrashort laser pulses', *Rep. Prog. Phys.*, **46**, 1983, pp. 877-971
- INABA, H.: 'Generation and control of transform limited optical pulses in subpico- and picosecond regions from semiconductor laser diodes', *Int. J. Electron.*, **60**, 1985, pp. 5-21
- CORZINE, S.E.W., BOWERS, J.E., PRZYBLEK, G., KOREN, U., MILLER, B.I., and SOCCOLICH, C.E.: 'Actively mode locked GaInAsP laser with subpicosecond output', *Appl. Phys. Letts.*, **52**, 1988, pp. 348-350
- TUCKER, R.S., EISENSTEIN, G., KOROTKY, S.K.: 'Optical time-division multiplexing for very high bit-rate transmission', *IEEE Trans.*, **LT-6**, pp. 1737-1749
- HARRIS, E.P.: 'Spiking in current-modulated cw GaAs external cavity lasers', 1971, *J. Appl. Phys.*, **42**, 1971, pp. 892-893
- HO, P.T., GLASSER, L.A., IPPEN, E.P., and HAUS, H.A.: 'Picosecond pulse generation with a cw GaAlAs laser diode', *Appl. Phys. Letts.*, **33**, 1978, pp. 241-242
- HAUS, H.A., and HO, P.T.: 'Effect of noise on active mode-locking of a diode laser', *IEEE Trans.*, **QE-15**, 1979, pp. 1258-1265
- HAUS, H.A.: 'A theory of forced modelocking', *IEEE Trans.*, **QE-11**, 1975, pp. 323-330
- HAUS, H.A.: 'Theory of modelocking of a laser diode in an external resonator', *J. Appl. Phys.*, **51**, 1980, pp. 4042-4049
- HAUS, H.A.: 'Models of mode-locking a laser diode in an external resonator', *IEE Proc. I*, **127**, 1980, pp. 323-329
- HAUS, H.A.: 'Mode-locking of semiconductor laser diodes', *Jap. J. Appl. Phys.*, **20**, 1981, pp. 1007-1020
- CHEN, J., and PAN, D.: 'A rate equation analysis of actively mode-locked semiconductor lasers', *IEEE Trans.*, **QE-22**, 1986, pp. 26-31
- VAN DER ZIEL, J.P.: 'Active mode-locking of double heterostructure lasers in an external cavity', *J. Appl. Phys.*, **52**, 1981, pp. 4435-4446
- AU YEUNG, J.: 'Theory of active mode locking of a semiconductor laser in an external cavity', *IEEE Trans.*, **QE-17**, 1981, pp. 398-404
- ASPIN, G.J., and CARROLL, J.E.: 'Simplified theory for mode locking in injection lasers', *Solid-State and Electron Devices*, **3**, 1979, pp. 220-223
- DEMOKAN, M.S.: 'A model of a diode laser actively mode-locked by gain modulation', *Int. J. Electron.*, **60**, 1986, pp. 67-80
- KEMPF, P., and GARSIDE, B.K.: 'Dynamics of mode-locked laser diodes employing a repetitive short-pulse drive current', *Appl. Optics*, **26**, 1987, pp. 4522-4527
- GOODWIN, J.C., and GARSIDE, B.K.: 'Modulation detuning characteristics of actively mode-locked diode lasers', *IEEE Trans.*, **QE-19**, 1983, pp. 1068-1073
- KELLY, S., NEW, G.H.C., and WOOD, D.: 'Mode-locking dynamics of synchronously-pumped colour-centre lasers', *Appl. Phys. B*, **47**, 1988, pp. 349-357

- 20 LOWERY, A.J.: 'New dynamic semiconductor laser model based on the transmission-line modelling method', *IEE Proc. J.*, **134**, 1987, pp. 281-289
- 21 LOWERY, A.J.: 'A new time-domain model for spontaneous emission in semiconductor lasers and its use in predicting their transient response', *Int. J. Numerical Modelling*, **1**, 1988, pp. 153-164
- 22 LOWERY, A.J.: 'A new inline wideband dynamic semiconductor laser amplifier model', *IEE Proc. J.*, **135**, 1988, pp. 242-250
- 23 LOWERY, A.J.: 'Transmission line modelling of semiconductor lasers', PhD Thesis, Nottingham University, 1988
- 24 HOEFER, W.: 'The transmission line matrix method theory and applications', *IEEE Trans.*, **MTT-33**, 1985, pp. 882-893
- 25 CHEN, J., SIBBETT, W., and VUKUSIK, J.I.: 'Tunable mode-locked semiconductor lasers incorporating brewster-angled diodes', *Optics Commun.*, **48**, 1984, pp. 427-431
- 26 PHELAN, P., and BRADLEY, D.J.: 'Hybrid mode-locking of an angled-stripe CCC laser', *Electron. Letts.*, **22**, 1986, pp. 738-740
- 27 AU YEUNG, J.C., BERGMAN, L.A., and JOHNSON, A.R.: 'Transient behaviour of actively mode-locked semiconductor laser diode', *Appl. Phys. Letts.*, **41**, 1982, pp. 124-126
- 28 VASIL'EV, P.P., MOROZOV, V.N., and SERGEEV, A.B.: 'Bandwidth-limited picosecond pulses from an injection GaAlAs DH laser with an external dispersive cavity', *IEEE Trans.*, **QE-21**, 1985, pp. 576-581
- 29 AU YEUNG, J.C., and JOHNSTON, A.R.: 'Picosecond pulse generation from a synchronously pumped mode-locked semiconductor laser diode', *Appl. Phys. Letts.*, **40**, 1982, pp. 112-114
- 30 TUCKER, R.S., KOROTKY, S.K., EISENSTEIN, G., KOREN, U., STULZ, L.W., and VESELKA, J.J.: '20 GHz active mode-locking of a 1.55 μm InGaAsP laser', *Electron. Letts.*, **21**, 1985, pp. 239-240
- 31 McINERNEY, J., REEKIE, L., and BRADLEY, D.J.: 'Bandwidth-limited picosecond pulse generation by hybrid mode-locking in a ring cavity GaAlAs laser', *Electron. Letts.*, **21**, 1985, pp. 117-118
- 32 DIMMICK, T.E., HO, P.-T., and BURDGE, G.L.: 'Coherent pulse generation by active modelocking of a GaAlAs laser in a SELFOC lens extended resonator', *Electron. Letts.*, **20**, 1984, pp. 831-833
- 33 TUCKER, R.S., EISENSTEIN, G., and KAMINOV, I.P.: '10 GHz active mode-locking of a 1.3 μm ridge-waveguide laser in an optical-fibre cavity', 1983, *Electron. Letts.*, **19**, 1983, pp. 552-553
- 34 Private Communication with I.W. Marshall, BTRL, Ipswich, U.K.